



## RESEARCH ARTICLE

# Silicon heterojunction solar cells toward higher fill factor

Luca Martini | Luca Serenelli | Francesca Menchini | Massimo Izzi | Mario Tucci

ENEA Research Centre Casaccia, Rome, Italy

**Correspondence**

Luca Serenelli, ENEA Research Centre Casaccia, via Anguillarese 301, 00123 Rome, Italy.  
Email: luca.serenelli@enea.it

**Funding information**

European Union, Grant/Award Number: 745601

**Abstract**

One of the most limiting factors in the record conversion efficiency of amorphous/crystalline silicon heterojunction solar cells is the not impressive fill factor value. In this work, with the aid of a numerical model, the ways to enhance the cell fill factor up to 85% are investigated in detail, considering the properties of conventional amorphous-doped films, wider Energy gap layers, and transparent conductive oxide films. The band alignment among the various materials composing the heterojunction is the key to high efficiency but becomes an issue for the solar cell fill factor, if not well addressed. One of the most interesting outcomes of this work is the evidence of hidden barriers arising between the transparent conductive oxide and both selective contacts, due to the mismatch between their work functions. The measurement of light current-voltage characteristics performed at low temperature is proposed as a way to identify the presence of these barriers in efficient solar cells that do not possess high fill factor values. Experimental J-V characteristics compared with numerical simulations demonstrated that the sometimes neglected cell base contact needs instead a more careful consideration. To this aim, a model to predict the presence of a hidden barrier at the base contact that limits the cell fill factor is proposed.

**KEY WORDS**

base contact, energy barrier, fill factor, heterojunctions, simulations, TCO

## 1 | INTRODUCTION

In the crystalline silicon solar cell market, the amorphous/crystalline silicon (a-Si:H/c-Si) HeteroJunction (HJ) technology is becoming more and more relevant, continuously attracting the attention of the researchers and industry. A typical structure of a HJ is sketched in Figure 1: the absorber is constituted by a n-type c-Si wafer, excellently passivated on both surfaces by intrinsic a-Si:H thin film. The selective contacts are obtained by two doped a-Si:H films, namely, p-a-Si:H and n-a-Si:H for the emitter and base contact, respectively. The low resistance contacts are ensured by the deposition of a Transparent Conductive Oxide (TCO) film followed by a screen printed silver grid on both sides to obtain a bifacial solar cell. The main advantages achievable by this technology comprise high efficiency, low thermal budget manufacturing steps, low degradation of n-type c-Si under sunlight, and low temperature coefficient of solar cell efficiency.

However, there are some drawbacks. One relevant limitation is the relatively low Fill Factor (FF) value of the current-voltage (J-V) characteristic under sunlight exposure, when compared with the state of the art of homojunction solar cells in which a FF value higher than 84% has been demonstrated.<sup>1</sup> Typical FF values for HJs are indeed in the range of 82–83.5%,<sup>2</sup> where the latter is related to the actual record HJ cell of 25.1% efficiency.<sup>3</sup> Such FF values are of course mainly limited by the low conductivity of silver grids produced by screen printing of pastes necessarily designed to harden and melt at temperatures below 200°C,<sup>4</sup> which have a conductivity one order of magnitude lower than that of the conventional pastes for homojunctions. Another resistive problem arises from the lateral transport in the TCO used to reduce the doped a-Si:H layers resistivity. However, the resistance is not the only problem that TCOs can introduce in the device efficiency. The carrier selectivity of the contacts has a very relevant role in the cell efficiency.<sup>5</sup> In HJ cells, the selectivity is ensured by

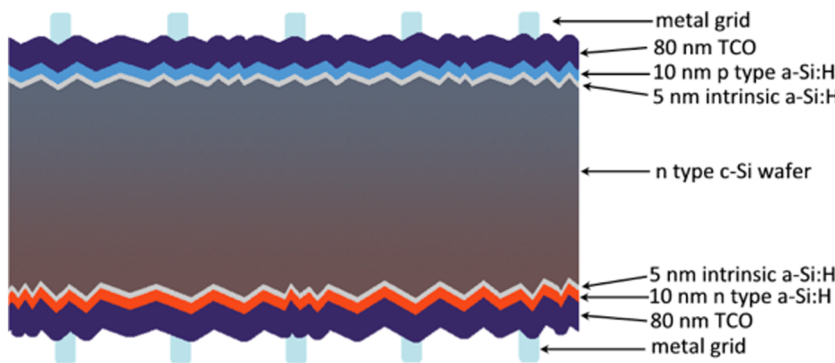


**FIGURE 1** Scheme of a bifacial a-Si:H/c-Si heterojunction solar cell

perfect surface passivation and energy band alignment among the layers at both emitter and base contacts. Nevertheless, the selective contacts alone are not sufficient to ensure the efficient carrier collection, due to the high resistivity of the a-Si:H doped films. TCO layers and metal electrodes to achieve efficient solar cells are necessary. Thus, in amorphous/crystalline silicon HJ solar cells, the energy band alignment among all the layers is the key to high efficiency but also the source of issues. Indeed, it has been recognized that the TCO work function ( $\Phi_{TCO}$ ) can play a role in this picture, introducing an undesired barrier to the charge extraction that can lead to FF reduction, with the formation of an S-shape in the J-V characteristics.<sup>6</sup> Several works reported in the literature suggest that this problem affects the emitter side of the HJ.<sup>7-9</sup> To better address the impact of the buffer/emitter layers on the cell FF, numerical simulations of the device are used,<sup>10,11</sup> starting from experimentally measured properties of the layers. Nevertheless, even the base contact contributes to the issue, the base contact on p-type c-Si obtained with intrinsic/p-doped a-Si:H is well known to introduce a valence band offset against hole-selective collection that can only be overcome by introducing a high doping level in the p-doped a-Si:H or by some particular laser treatments.<sup>12</sup> On the other hand, in principle, the ohmic contact on n-type c-Si is easier to produce, because of a lower barrier with the n-doped a-Si:H at the conduction band edge.<sup>9</sup> However, the work function of the TCO deposited above this doped layer is not always carefully considered, even because at room temperature, it is difficult to immediately recognize any barrier issue when the cell FF range around 80%. Instead, only the resistive aspect of the contacts and metal electrodes is addressed in order to gain FF and cell efficiency. To definitively evaluate the hidden issues, light J-V characteristics at decreasing temperatures are measured and discussed with the aid of a numerical model to find a correlation between the cell FF reduction and the shape of the J-V characteristics. From these observations, it is now evident how some barriers arising at low temperatures and almost hidden at room temperature are still limiting the cell FF, with a not negligible effect.

## 2 | NUMERICAL SIMULATIONS OF HJ SOLAR CELLS

To address the FF issue in HJ and suggest solutions, numerical simulations of the solar cell device can be an option. To this aim, a

monodimensional description of the device along its thickness is followed, which is mainly preferred due to the homogeneity of the crystalline silicon absorber along the other two dimensions under the practical hypothesis of high-quality monocrystalline silicon.<sup>10</sup> Also, the thin films composing the buffer layer and both base and emitter contacts can be considered as homogeneous along the other two physical dimensions. This was practically demonstrated, even at industrial level, and can be achieved, thanks to the Plasma Enhanced Chemical Vapor Deposition (PECVD) systems commonly used to manufacture such thin films and able to produce high HJ solar cell performances. Therefore, the approach used for the numerical simulations of the HJ solar cells is based on two fundamental hypotheses summarized as follows:

1. Description of the interfaces under the Anderson hypothesis, assuming that each surface has the same intrinsic properties of the bulk, such as Energy gap and electron affinity.<sup>13</sup>
2. High-quality homogenous c-Si substrate with a very low density of defects at midgap (lower than  $10^{11} \text{ cm}^{-3}$ ).

Several numerical simulators are available to describe the carrier transport along the stacked structure of a device such as a solar cell. We have preferred a homemade numerical simulator for the sake of familiarity,<sup>10</sup> but it is worth noting that very similar results to those presented can be obtained with other available numerical simulators.

The numerical simulator adopted in this work solves the Poisson, continuity, and current equations under bias condition, temperature, and light exposure, dividing the device structure in a stack of sub-layers. In particular, 60 stacked sublayers are used to discretize the device: 40 of these to discretize the two anterior and posterior heterostructures and 20 to discretize the bulk silicon. This mesh ensures a more accurate spatial description of the most relevant parts of the device. Each layer is described by a set of parameters including type and concentration of dopant, free carrier mobility ( $\mu$ ) for electrons and holes, electron affinity ( $\chi$ ), Energy gap ( $E_g$ ), Density Of States distribution (DOS), and capture cross section for electrons and holes.

For the a-Si:H materials, this distribution is necessary to describe the effects of weak-bonds and dangling-bonds that affect the disordered amorphous network. The weak-bonds are considered as shallow defects in the energy gap and are commonly described by two band tails exponentially dropping from the edges of both conduction and valence bands toward the midgap of the forbidden band. The

bending of these distributions is parameterized by the temperature  $T_{c,v}$  (ie,  $\exp(E/kT_{c,v})$ ), and the capture cross section of these states is indicated by  $C_{n,p}^{\text{tail}}$ . From the literature on a-Si:H films, 350 and 500 K are widely accepted values for the temperatures of conduction and valence band tail distribution, respectively. Taking into account that the SiO<sub>x</sub>:H film (later reported in this work) has amorphous network quite similar to the a-Si:H film, the same tail values have been assumed also for SiO<sub>x</sub>:H films. The dangling-bonds are instead described as at least two Gaussian distributions of states within the gap. Each of them is parameterized by amplitude ( $N_{db}$ ), distribution center ( $E_0$ ), and standard deviation ( $\sigma$ ), and the acceptor or donor-like behaviour of the state is defined by their capture cross section ( $C_n$ ,  $C_p$ ) values. The centre of the donor-like (d) states Gaussian distribution is positioned with respect to the centre of acceptor-like (a) states in order to simulate the amphoteric behaviour of the dangling-bond defect. A cross-section difference of at least two orders of magnitude is imposed to underline the different behaviour between shallow and deep defects. In Table 1, the list of parameters used to simulate the DOS of un-doped and doped amorphous films is reported. Doped films are simulated by enhancing the density of states and introducing into the forbidden gap a distribution centred sufficiently close to the band to ensure an  $E_d$  equal to that experimentally measured. Instead, c-Si is simulated by letting the forbidden band almost empty (less than  $1 \times 10^{11} \text{ cm}^{-3}$ ), except for the doping distribution kept to ensure the wafer conductivity and doping type. Numerical solutions give, in each layer and at each temperature and illumination, the density of free and trapped carriers, the values of electric field, and potential. Generation and recombination rates are calculated following the Shockley-Hall-Read theory. As boundary conditions at the two metals, used as front and back contact respectively, no variation of the free carriers is imposed.<sup>10</sup>

**TABLE 1** Parameters used to simulate the DOS within the forbidden band of amorphous films

Film	$T_c$ , K	$T_v$ , K	$C_{n,p}^{\text{tail}}$ , $\text{cm}^3/\text{s}$	$E_{0a}$ , eV	$\sigma_a$ , eV	$N_{dba}$ , $\text{cm}^{-3}$	$C_{n,pa}$ , $\text{cm}^3/\text{s}$	$E_{0d}$ , eV	$\sigma_d$ , eV	$N_{dbd}$ , $\text{cm}^{-3}$	$C_{n,pd}$ , $\text{cm}^3/\text{s}$
a-Si:H	350	500	$1 \times 10^{-13}$	0.91	0.1	$1 \times 10^{15}$	$1 \times 10^{-9}, 1 \times 10^{-8}$	0.81	0.1	$1 \times 10^{15}$	$1 \times 10^{-8}, 1 \times 10^{-9}$
a-Si:H <sub>p,n</sub>	350	500	$1 \times 10^{-13}$	0.91	0.1	$1 \times 10^{16}$	$1 \times 10^{-9}, 1 \times 10^{-8}$	0.81	0.1	$1 \times 10^{16}$	$1 \times 10^{-8}, 1 \times 10^{-9}$
SiO <sub>x</sub> :H	350	500	$1 \times 10^{-13}$	1.07	0.1	$1 \times 10^{16}$	$1 \times 10^{-9}, 1 \times 10^{-8}$	0.91	0.1	$1 \times 10^{16}$	$1 \times 10^{-8}, 1 \times 10^{-9}$
SiO <sub>x</sub> :H <sub>p,n</sub>	350	500	$1 \times 10^{-13}$	1.07	0.1	$1 \times 10^{16}$	$1 \times 10^{-9}, 1 \times 10^{-8}$	0.91	0.1	$1 \times 10^{16}$	$1 \times 10^{-8}, 1 \times 10^{-9}$

**TABLE 2** Parameters experimentally determined for the materials used in the numerical simulations of the solar cells

Material	$E_g$ , eV	$\mu_{n,p}$ , $\text{cm}^2/\text{Vs}$	$\chi$ (eV)	$E_{d,n,p}$ , eV	Thickness
c-Si	1.124	1417–470	4.05	0.175	160 $\mu\text{m}$
i a-Si:H	1.72	1–0.1	3.9		5 nm
n a-Si:H	1.72	1–0.1	3.9	0.17	15 nm
p a-Si:H	1.72	1–0.1	3.9	0.42	5 nm
i SiO <sub>x</sub> :H	1.95	5–0.5	3.9		5 nm
n SiO <sub>x</sub> :H	1.95	5–0.5	3.9	0.05	15 nm
p SiO <sub>x</sub> :H	1.95	5–0.5	3.9	0.50	5 nm
p <sup>+</sup> SiO <sub>x</sub> :H	1.95	5–0.5	3.9	0.18	5 nm

To simplify the description, the density of states at the interface between the a-Si:H buffer layer and c-Si is integrated along the thickness of the buffer layer and then reported as  $D_{it}$  ( $\text{cm}^{-2}$ ).

Most of the intrinsic properties of any material used in the device simulations, such as  $E_g$ ,  $\mu$ ,  $\chi$ , optical absorptions, and refractive indexes, are deduced from experimental measurements and are listed in Table 2. In Figure 2, the absorption coefficients and the refractive indexes of the materials used in the numerical simulations (c-Si, a-Si:H, and SiO<sub>x</sub>:H deposited as described in another work<sup>14</sup>) are deduced from reflectance and transmittance spectroscopy and ellipsometric measurements, respectively, and then compared. The same approach is used for some extrinsic properties, such as the doping activation energy ( $E_d$ ) for both n- and p-type-doped films and film thicknesses. However, the densities of states within the Energy gap of thin film materials are assumed on the base of literature values and are also used as free parameters within a reasonable range.

Due to the large number of free parameters present in the description of a HJ solar cell device, it is not easy to determine the right set of values that can represent a very efficient solar cell replicable in practice. The solar cell FF represents the most relevant photovoltaic parameter because it is immediately related to the power available from the solar cell generator and it depends on the physical characteristics of each material composing the device and to carrier transport at the junction and collection at the electrodes. Therefore, the FF values are assumed to summarize the effectiveness of a solar cell device.

To focus the numerical simulations on the solar cell FF, a top-down approach is used, starting from an optimal solar cell with efficiency very close to the physical limit achievable with the a-Si:H/c-Si HJ technology (a little higher than the actual world record

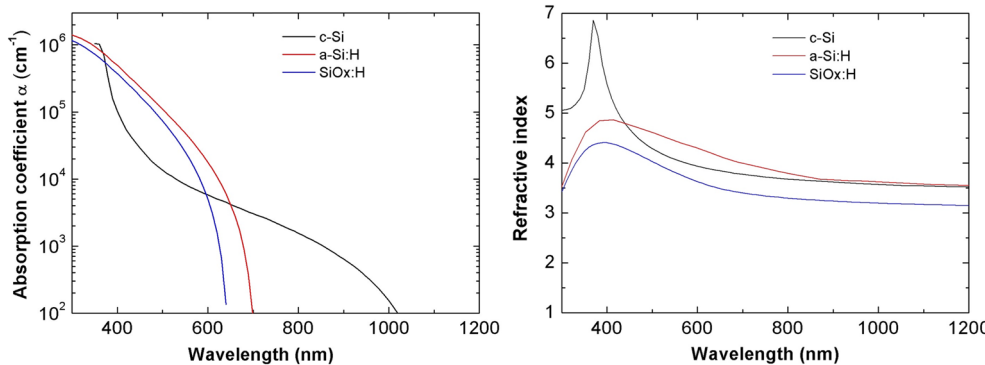


**FIGURE 2** Absorption coefficients of materials used in the numerical simulations, as experimentally deduced from reflectance and transmittance measurements (left). Refractive indexes of materials used in the numerical simulations, as experimentally deduced from ellipsometric measurements (right)

efficiency for a transverse structure similar to that under simulation), in which all the free parameters are assumed to be close to their physical limit value. Then, each of these parameters is varied and the corresponding FF variation is monitored. Figure 3 summarizes and compares the light J-V characteristics of the former and actual record HJ cells,<sup>3,16</sup> the theoretical limit (intrinsic radiative Auger recombination) of a silicon based cell fabricated on a 100- $\mu$ m-thick textured c-Si substrate,<sup>15</sup> and the reference best HJ cell (used as “starting point”) of the numerical simulations proposed in this work and based on the 160- $\mu$ m-thick c-Si wafer as actually used for the HJ state of the art at industrial level.

In Table 3, the photovoltaic parameters of the HJ cells of Figure 3 are listed. It is worth noting that the  $J_{sc}$  value of the theoretical limit cell is assumed to be not shadowed by any front metal grid, while for the starting point HJ, a 5% front shadowing is considered.

The energy band distribution of the starting point HJ cell in dark and light at 0 V bias as deduced from numerical simulations is

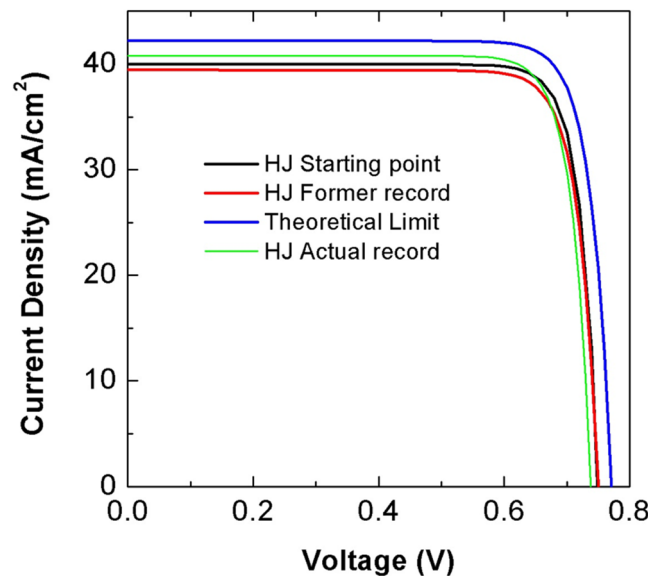


**FIGURE 3** Comparison between light J-V characteristics of heterojunction solar cells: The blue line is the theoretical limit for c-Si-based solar cells,<sup>15</sup> the red line is the 24.7% HJ former record,<sup>16</sup> the green line is the 25.1% HJ actual record,<sup>3</sup> and the black line is obtained from the simulation with the proposed parameters and is the starting point for the analysis

reported in Figure 4, together with recombination along the device, electron ( $n$ ), and hole ( $p$ ) distributions with a focus on the interfaces.

As evident from the Fermi level position at the a-Si:H p/i/n c-Si interface, the p-n junction is induced within the silicon substrate. This effect is also confirmed by the excess hole distribution at the same interface within the n c-Si. This equilibrium condition is helpful to keep the Fermi level away from the midgap position at the heterointerface, thus reducing the impact of recombination on the  $V_{oc}$  value of the HJ cell. Moreover, the presence of a valence band offset does not impose a strong limitation to hole collection at the emitter side due to the presence of the built-in voltage and the electric field. On the rear side of the cell, where the base contact lays, the small accumulation of electrons at the heterointerface ensures the effectiveness of the base contact, while the valence band offset strongly contributes to keep the holes away from the electron collection point. In Figure 4, the density of states distribution in the a-Si:H buffer layers on both sides of the solar cell, corresponding to  $D_{it} = 1.25 \times 10^9 \text{ cm}^{-2}$ , is reported. The thicknesses and the doping activation energy  $E_d$  of each layer used in the simulation are listed in Table 2. In particular, the  $E_d$  of n-type doped c-Si refers to a 1 Ω·cm, 160- $\mu$ m-thick n-type doped wafer. The simulations in light condition are performed by illuminating the device from the emitter side, as commonly done to achieve the record efficiency.<sup>2</sup> In the following, several parameters are varied from the starting point HJ and the effect is monitored in terms of cell FF variation.

## 2.1 | Emitter thickness

To reduce the undesired effect of parasitic absorption of the emitter and buffer layer at the HJ cell front side, one approach could be the reduction of both thicknesses. However, as widely known, the buffer layer cannot be reduced below 5 nm to avoid the reduction of crystalline silicon surface passivation.<sup>14</sup> Instead, the effect of emitter thickness reduction on the cell FF is evident from the data reported in Figure 5. In particular, the thinner the emitter layer is, the higher the cell FF results; the effect is mainly due to the reduction of the series resistance contribution related to the low conductivity of the emitter layer of the p-type doped a-Si:H film. Nevertheless, in practice, the emitter thickness should prudentially not be thinner than 5 nm to

**TABLE 3** Photovoltaic parameters of the HJ cells

Solar cell	$J_{sc}$ , mA/cm <sup>2</sup>	$V_{oc}$ , mV	FF, %	Eff, %	Thickness, μm
Theoretical limit	42.2 (total area)	770	86.0	28.0	100
HJ former record	39.5 (total area)	750	83.2	24.7	100
HJ actual record	40.8 (aperture area)	738	83.5	25.1	160
HJ starting point	40.0 (total area)	750	84.5	25.3	160

avoid incomplete coverage of the cell surface, especially when the c-Si surface is textured.

## 2.2 | Density of states at the interface

As expected, when the density of states at the heterointerface close to the emitter side increases, the FF decreases. In particular, a  $D_{it}$  lower than  $5 \times 10^9$  cm<sup>-2</sup> must be achieved in the a-Si:H buffer layer used for surface passivation of the c-Si to ensure a cell FF as high as 84% and consequently a high efficiency solar cell. The  $D_{it}$  of course still remains the most relevant concern in the entire HJ fabrication procedure. As seen from Figure 6, the cell FF dependence from  $D_{it}$  is strongly nonlinear. Therefore, a strong effort to clean the c-Si surface and perfectly passivate it is definitively required to achieve record efficiencies. In the numerical simulation, the buffer thickness has been fixed on the basis of literature values.<sup>17</sup>

## 2.3 | Emitter doping

One of the a-Si:H layer limitations is the p-type doping efficiency that, contrary to that of n-type, does not allow the achievement of  $E_d$  as low as 0.35 eV on layers definitively thicker than those used as a front side emitter in HJ applications.<sup>18</sup> Indeed, in this case, to avoid undesired parasitic absorption of light impinging onto a solar cell, the emitter layer should be as thin as possible, as already seen in the previous paragraph. However, the emitter layer cannot be thinned too much because the contact with TCO tends to undesirably deplete it. Therefore, in the proposed numerical simulations, the  $E_d$  of the p-doped layer is deliberately kept not lower than 0.4 eV on a 5 nm thin emitter layer; otherwise, the results could not be compared with the practical experience. Nevertheless, as evident from data reported in Figure 7, if the p-type doped emitter layer achieved an  $E_d = 0.4$  eV, the cell FF would reach 85%, and at the same time, the  $V_{oc}$  of the cell would assume the record value of 770 mV. Moreover, it is also evident how sensitive the FF and the  $V_{oc}$  are to small variations of doping.

## 2.4 | Valence band offset

Looking at the band diagram reported in Figure 4, it is quite evident that the valence band offset  $\Delta E_V$  at the heterointerface represents an

issue to hole collection toward the emitter.<sup>19</sup> It is worth noting that all the simulations are performed using only the thermionic emission contribution to overcome the barrier, in order to evaluate the possibility to collect the holes without the aid of any tunnelling mechanism. On the other hand, a tunnelling mechanism could only enhance the transport and not reduce it. Therefore, as expected, the higher the band offset is, the lower the cell FF results, as reported in Figure 8. Nevertheless, the possibility to overcome this issue is related to the electric field at the HJ, which, in turn, is influenced by the built-in voltage. This latter depends on the  $E_d$  of the emitter layer, but unfortunately, the p-type-doped a-Si:H cannot be overdoped to reduce the  $E_d$ , as already mentioned in the previous paragraph. Therefore, the only way to overcome this issue is to replace the p-type-doped a-Si:H emitter with a different material, which can be more heavily doped, still maintaining similar band alignment at the heterointerface.

This result suggests, in principle, that any increment of  $\Delta E_V$  should be avoided in order to ensure high cell efficiencies. Therefore, any wider gap material, as, for example, SiOx:H (SiOx in the following) or a-SiC:H, which are able to reduce or solve the undesired parasitic absorption of the amorphous front layer, should be avoided, as they would increase the  $\Delta E_V$ . Indeed, from the numerical simulations, if the front p/i a-Si:H emitter and passivation layers are replaced by wider gap p/i SiOx layers, respectively, the light J-V characteristic shows a pronounced FF reduction, as reported in Figure 9 in comparison with the starting point HJ cell. Nevertheless wide gap emitter/buffer layers can still be used if the two different strategies described below to escape from cell FF undesired reduction are adopted:

1. An emitter more highly doped than the a-Si:H counterpart. In this case, a higher built-in potential occurs, thus helping to overcome the barrier against holes collection. The energy band distribution due to this effect is reported in Figure 10(A), in which the two different situations of lower and higher emitter doping based on the  $E_d$  reported in Table 2 are compared. In practice, the use of p/i SiOx instead of p/i a-Si:H can be acceptable because the  $E_d$  of doped SiOx is definitively lower than that of the a-Si:H counterpart, as reported in the literature.<sup>20,21</sup> In Figure 9, the light J-V characteristic of a HJ cell with p<sup>+</sup>/i SiOx layers is reported. Due to the wider gap, a higher  $J_{sc}$  value is obtained, and a higher  $V_{oc}$  results due to a higher built-in voltage at the junction.
2. A buffer layer with graded  $E_g$  (ie, first layer of a-Si:H followed by SiOx). In this case, a double step gap (or graded gap) can promote the thermionic emission of holes over the barrier. In Figure 10(B), the energy band distribution of the conventional p/i a-Si:H layers

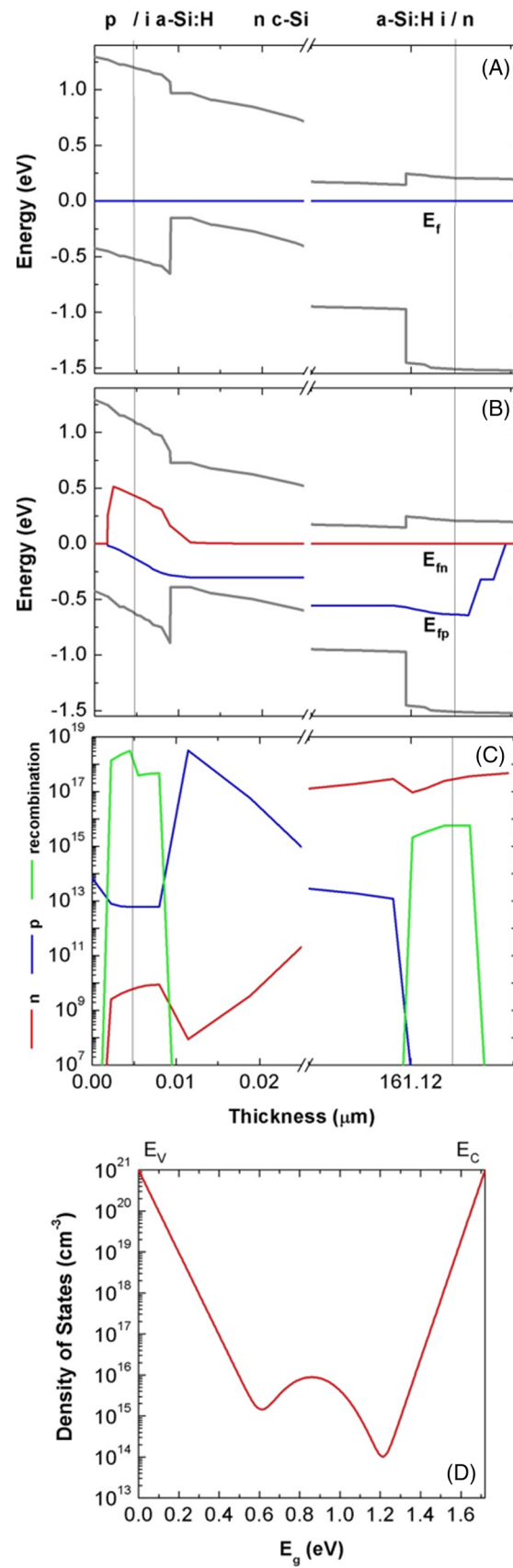


**FIGURE 4** Energy band distribution of the starting point heterojunction solar cell in dark (A) and light (B) at 0 V bias. The blue line is the Fermi level for holes, and the red line is the Fermi level for electrons. (C), electron ( $n$ ), hole ( $p$ ), and recombination distributions along the device at 0 V and light conditions. (D), density of states distribution in the a-Si:H buffer layers

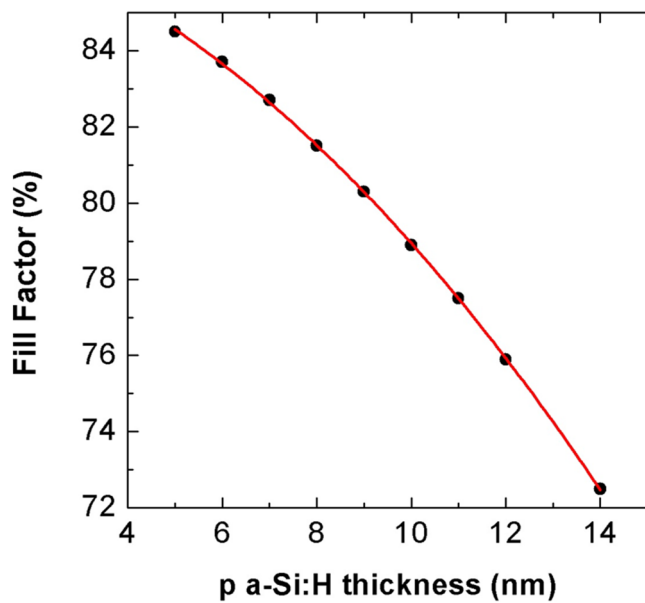


**FIGURE 5** Variation of the heterojunction cell fill factor as a function of the p-type a-Si:H layer thickness (the red curve is a guideline)

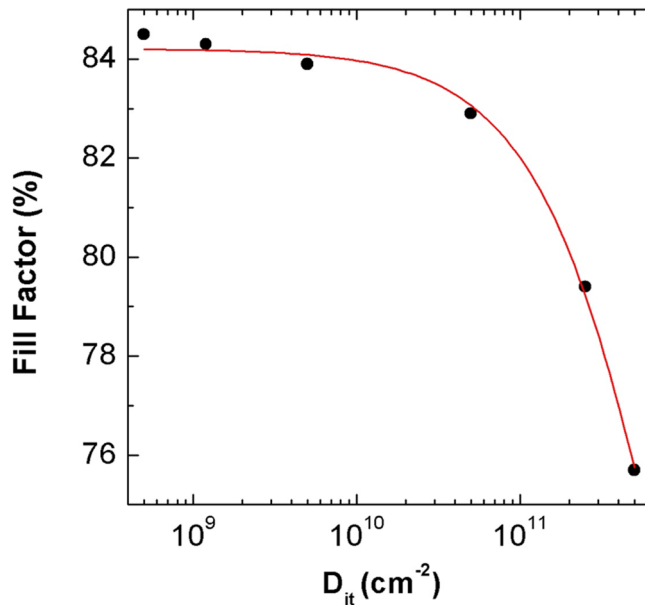


**FIGURE 6** Fill factor of the heterojunction cell as a function of  $D_{it}$  at the heterointerface close to the emitter side (the red curve is a guideline)

is compared with that of the more transparent p/i SiO<sub>x</sub> in which the first 2 nm of the SiO<sub>x</sub> buffer are assumed to have a bandgap as low as the one of the a-Si:H film.

In practice, the helpful graded bandgap is spontaneously formed when a SiO<sub>x</sub> buffer is deposited on a c-Si wafer because the SiO<sub>x</sub> film is a mixed phase material and the first layers of the film grown on c-Si are more hydrogenated than oxidized, to achieve effective surface

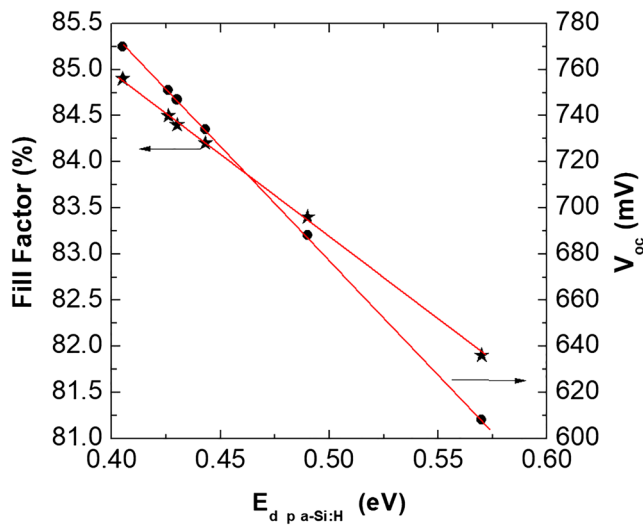


**FIGURE 7** Variation of the heterojunction cell fill factor and  $V_{oc}$  as a function of the  $E_d$  of the emitter layer (the red lines are guidelines)

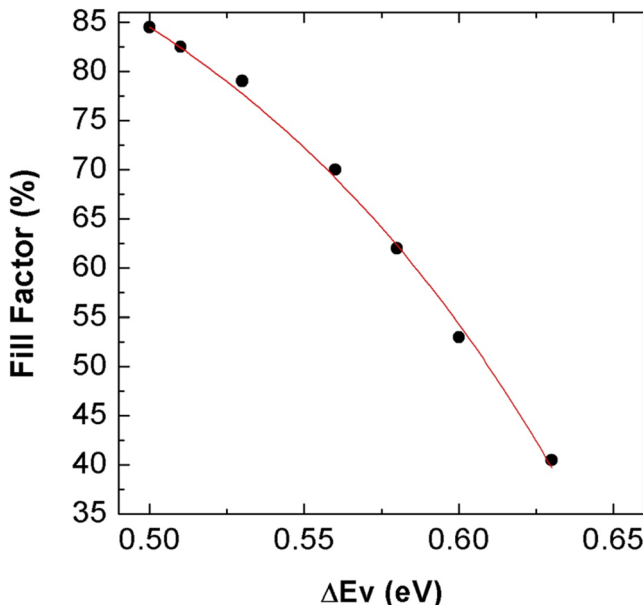


**FIGURE 8** Variation of the heterojunction cell fill factor as a function of  $\Delta E_v$  at the heterointerface close to the emitter side (the red curve is a guideline)

passivation. Therefore, they are more similar to an a-Si:H film than to a SiO<sub>x</sub> one.<sup>22</sup> In Figure 9, the light J-V characteristic of a HJ cell with p/i SiO<sub>x</sub>/i a-Si:H layers is then reported. Also, in this case, a higher  $J_{sc}$  value is obtained and a higher  $V_{oc}$  results, due to a higher built-in voltage at the junction.

## 2.5 | TCO work function

The TCO is necessary to overcome the issue of low conductivity of the a-Si:H doped layers and to reduce the specific contact resistivity

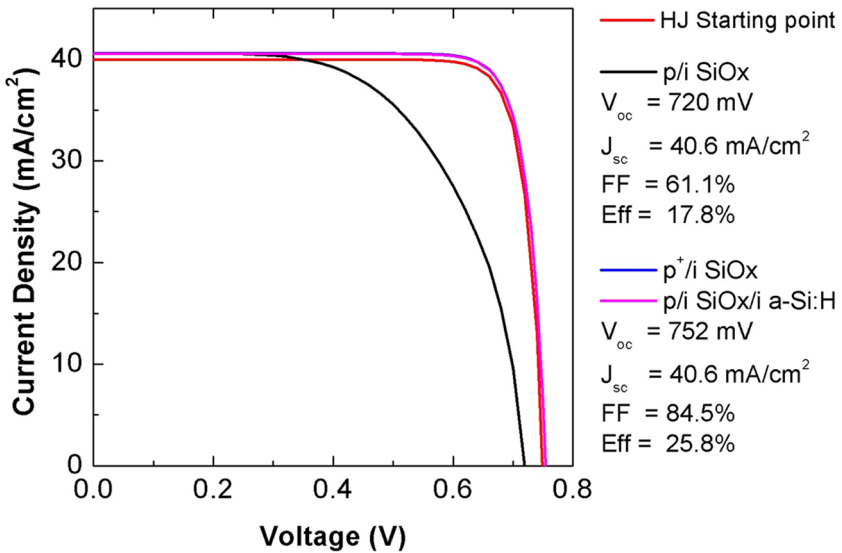


**FIGURE 9** Comparison between the light J-V characteristics obtained by simulation of the same structure but with different  $E_g$  and doping level in the window layer

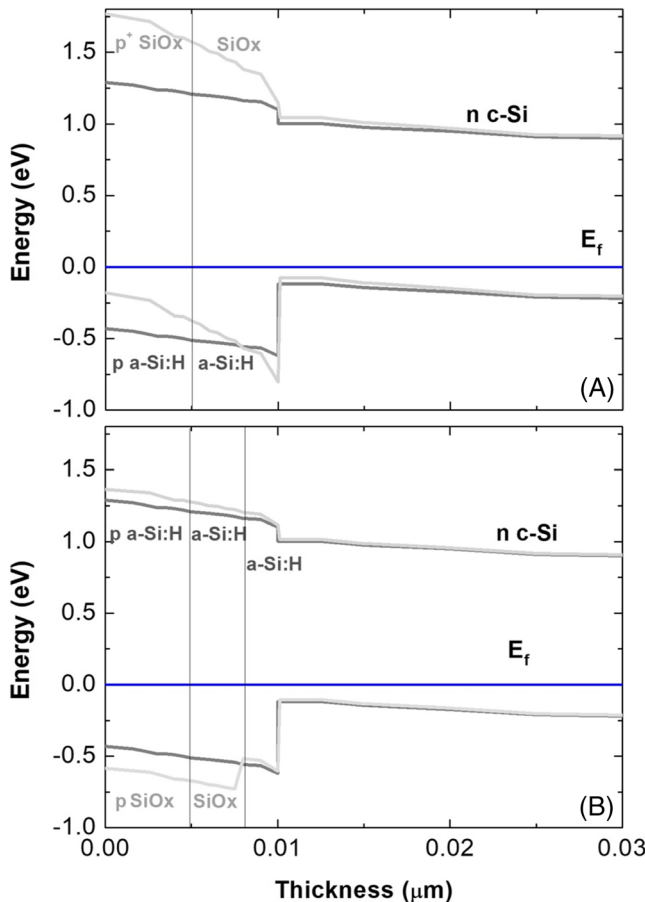


**FIGURE 10** Comparison of energy band distributions as deduced from numerical simulations: (A), p/i a-Si:H/n c-Si (gray lines), p<sup>+</sup>SiOx/i SiOx/n c-Si (light gray lines); (B), p/i a-Si:H/n c-Si (gray lines), p SiOx/i SiOx/i a-Si:H/n c-Si (light gray lines)

of the metal contact with both emitter and base layers. On n-type a-Si:H base contacts, the TCO basically does not represent a particular issue because any TCO layer is n-type doped and its role is just to

ensure an equipotential surface at the base contact. Instead, on a p-type-doped emitter, the situation is different, because in this case, the contact between TCO and emitter works as a tunnel contact. For the tunnelling to be effective, the barrier at the TCO/emitter interface must be very thin, and to this end, the emitter should be heavily doped to avoid the large emitter depletion, which would reduce the tunnelling mechanism.<sup>9,22</sup> In principle, the best solution should be the use of two different degenerate TCO layers: one with a high work function ( $\Phi \approx 5.2$  eV) on the emitter side and another with a lower work function ( $\Phi \approx 4.1$  eV) at the base contact, in order to respectively collect holes and electrons without affecting the Fermi level position at the edges of the cell. This situation is depicted in the energy band distribution of the HJ cell, deduced from numerical simulations, with the two degenerate TCOs at the edges, reported in Figure 11 (left). Nevertheless, it is very difficult to find in practice an effective TCO with a work function as high as 5.2 eV and an electron affinity value similar to the work function. If this condition is not accomplished, the p-type a-Si:H emitter depletes, due to the conduction band alignment at the edge of TCO and emitter layers, as calculated from numerical simulation of the band bending at the TCO/emitter interface and reported in Figure 11 (right).

In this case, the TCO is assumed to have  $\chi \approx \Phi = 4.4$  eV on both sides of the HJ cell, as typically obtained using an Indium Tin Oxide (ITO) layer. To slightly increase this value, it is preferable to deposit the TCO layer at room temperature, while, to reduce it, it is better to rise the temperature during the TCO deposition process. Also, on the base contact, the  $\Phi_{TCO}$  can be critical if higher than the Fermi level position in the n-type-doped a-Si:H layer. In Figure 11 (right), the formation of a small barrier at the n a-Si:H/TCO interface is evident when the TCO has  $\chi \approx \Phi = 4.4$  eV. This barrier is not as critical as the one formed at the emitter side, but if increased, it can promote depletion up to the n c-Si, leading to the formation of a larger barrier against electron collection. In Figure 12(A), the effect of the TCO with  $\Phi_{TCO} = 4.4$  eV on both sides on the light J-V characteristic of the HJ solar cell is reported with respect to the that of the starting point HJ

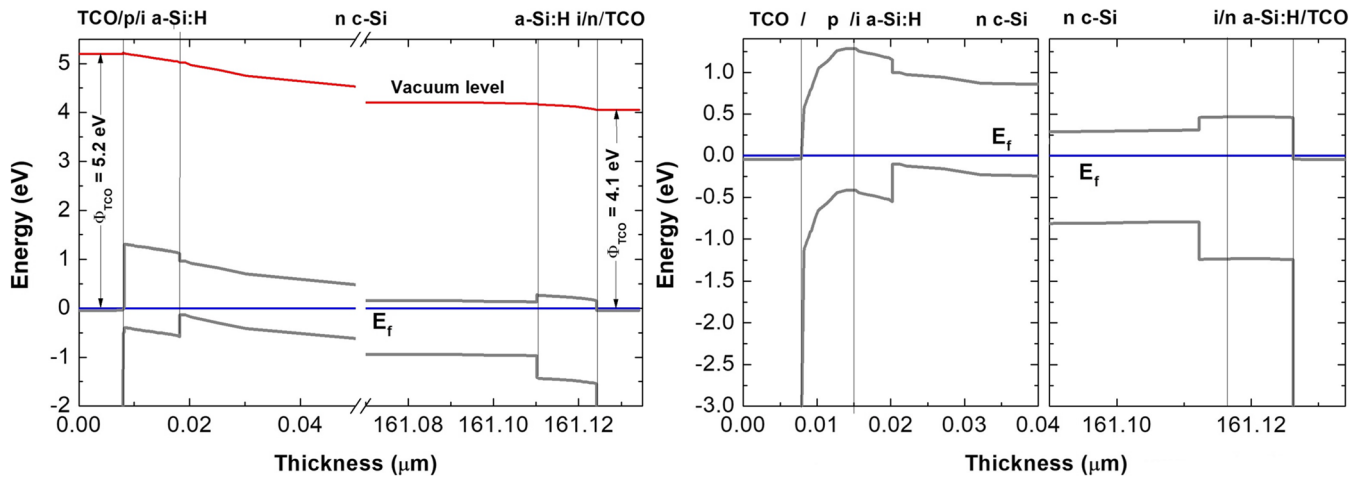


**FIGURE 11** Energy band distribution of the HJ solar cell with two different transparent conductive oxides (TCOs) at the edges in dark at 0 V bias (left). Emitter depletion and base depletion toward the TCO when both  $\Phi_{TCO}$  are equal to 4.4 eV (right). The blue line indicates the Fermi level

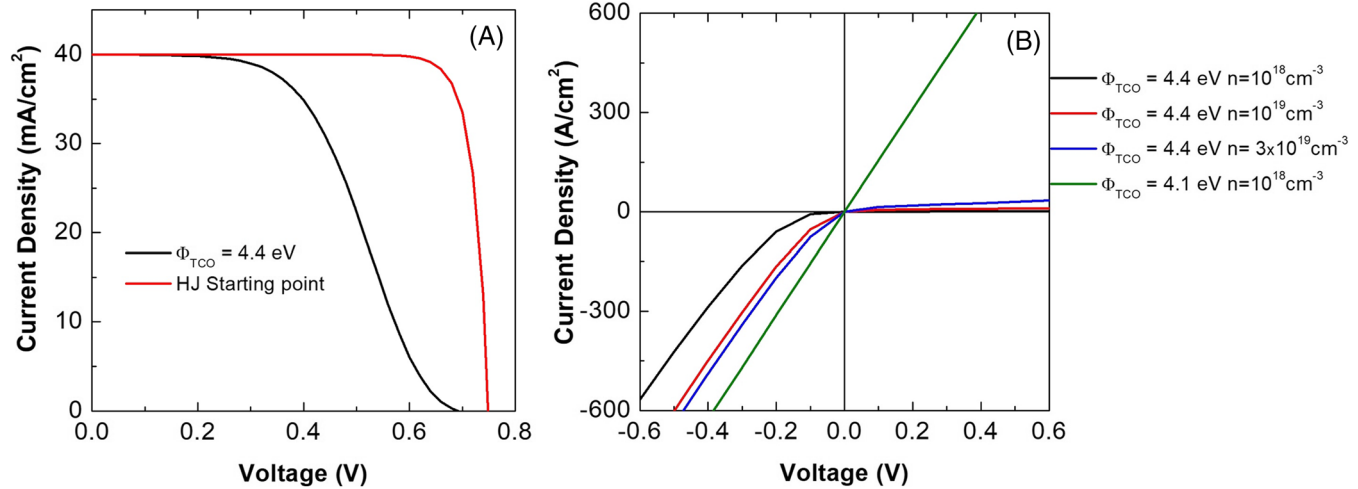


**FIGURE 12** (A) Simulated light J-V characteristics with a nonoptimal value of the  $\Phi_{TCO}$  on both sides of the cell. (B) Simulated J-V characteristics of the base contact as a function of doping and different  $\Phi_{TCO}$

cell. It is evident that the J-V characteristic is affected by an S-shape that reveals a barrier against carrier collection.

The numerical simulation of the J-V characteristic related to the rear side of the cell, obtained after removing the emitter, shows a behaviour that is not resistive or ohmic, but unexpectedly rectifying. This rectifying behaviour remains almost unchanged even after increasing the doping of the n a-Si:H layer. The only way to obtain a completely resistive behaviour is to reduce the  $\Phi_{TCO}$ , as reported in Figure 12(B). Thus, the undesired S-shape on the J-V characteristic can be also due to the base contact.

In conclusion, the emitter layer should be sufficiently doped to contribute to the thermionic emission of holes over the band bending mismatch  $\Delta E_V$  at the a-Si:H/c-Si interface and to avoid any depletion induced by the TCO. Moreover, also, the base contact must be optimized to avoid an undesired barrier against electron collection, with a particular focus on the  $\Phi_{TCO}$ .

### 3 | HIDDEN BARRIERS IN HJS

In this section, a method to discover hidden barriers in the HJ solar cell is suggested. As already illustrated, these barriers, mainly arising from misalignments of electron affinities and work functions at the TCO/a-Si:H/c-Si interfaces, contribute to produce cell FF values lower than expected.

The proposed method consists in measuring the J-V characteristic of the HJ cell under illumination and at different temperatures. Since very low temperatures are required, the measurements are performed in a cryogenic system (liquid nitrogen is used) equipped with an optical window to illuminate the sample so to obtain the same  $J_{sc}$  value measured under the sun simulator. The cryogenic system is kept under vacuum by a turbo-molecular pump ensuring a base vacuum of  $10^{-5}$  mbar. To ensure thermal and electric contact, the sample is held on a copper plate that is cooled with liquid nitrogen down to 80 K.

Solar cells used in this experiment have been produced starting from textured, 1 to 2 Ω·cm resistivity, 160-μm-thick FZ n-type wafers. The substrates have been cleaned according to a standard cleaning procedure<sup>23</sup> and dipped in 1% diluted HF just before being loaded into the PECVD reactor. A 5-nm-thick, intrinsic a-Si:H layer has been deposited on both sides of the wafer, then p-type and n-type-doped amorphous silicon layers have been deposited on the two faces in a three-chamber 13.56-MHz PECVD system, as already described in another work.<sup>18</sup> Subsequently, an 80-nm-thick ITO layer has been deposited on both emitter and base contacts at 60 W RF power. A metal grid has been finally produced on both cell sides by screen printing of low-temperature sintering commercial silver paste, cured at 180°C for 30 minutes.

The J-V characteristic of solar cells under both light and dark conditions are collected with the aid of a Keithley 236 electrometer. Figure 13(A) shows the light J-V characteristic of the HJ bifacial solar cell measured in the temperature range between 80 and 360 K, in steps of 10 K. The light is shone only on the emitter side of the cell. When the temperature is raised over 300 K, the J-V characteristic shows the expected  $J_{sc}$  enhancement and  $V_{oc}$  reduction, still maintaining high cell FF. Instead, after the temperature is reduced below 300 K, an undesired S-shape appears, becoming more pronounced at 80 K. This effect remarks that linear contributions, such as those due to the resistivity of doped layers, TCO, and metals and to contact resistivity between them, are not sufficient on their own to justify the low FF value, which is instead related also to hidden non-linearity as induced by work function mismatch. For comparison, in Figure 13(B), the light J-V characteristics of a conventional silicon-based homojunction are reported. The short circuit current in the J-V curves in Figures 13(A) and 13(B) follows the predictable values for a solar cell that is not affected by any S-shape; therefore, only resistivity effects dominate the cell FF.

The  $J_{sc}$  reduction as a function of the reduced temperature follows the energy gap  $E_g$  reduction of the c-Si absorber layer according to the equation

$$J_{sc}(T) = J_0 e^{\left(\frac{\beta^2(a-E_g(T))^2}{a}\right)} \quad (1)$$

where

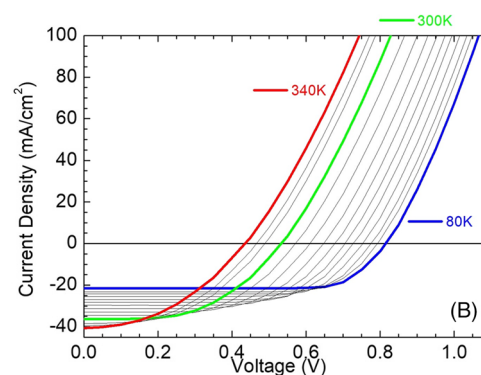
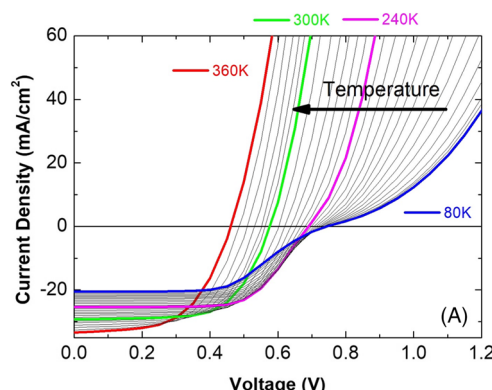


**FIGURE 14**  $J_{sc}$  of the heterojunction cell as a function of temperature. The dots are the experimental data; the red curve is derived from the theoretical model of equation (1)

$$E_g(T) = 1.1557 - \frac{T^2 \cdot 6.021 \cdot 10^{-4}}{T + 1108} \quad (2)$$

$J_0$  and  $\beta$  are two constants and  $\alpha$  is the absorption coefficient of the c-Si substrate. The temperature dependence of the  $E_g$  of the c-Si absorber substrate is written according to the literature.<sup>24,25</sup> The theoretical  $J_{sc}$  reduction is in good agreement with the experimental data, as reported in Figure 14, thus confirming that the  $J_{sc}$  is not affected by the S-shape.

At room temperature, the HJ cell works well even with a not excellent FF value. The barrier generating the S-shape at low temperature could be due to the emitter side of the cell or to the base contact. It is not easy to establish the main responsible but it is possible to determine which by exclusion.

Concerning the base contact, it is well known that for n-type c-Si-based HJ, it is straightforward to obtain a selective electron contact with an ohmic behaviour because of the small conduction band offset at the heterointerface between a-Si:H and c-Si ( $\approx 0.15$  eV).<sup>9</sup> Nevertheless, this is not completely true when a TCO layer is imposed to extract electrons from the n-doped a-Si:H layer, as already mentioned in the previous sections. Indeed, a higher value of the  $\Phi_{TCO}$  with

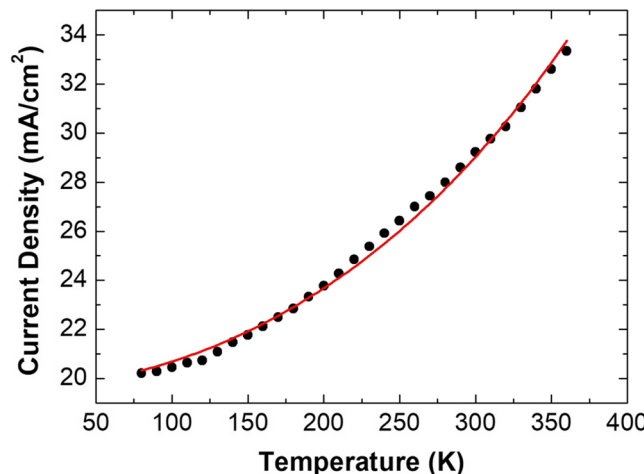


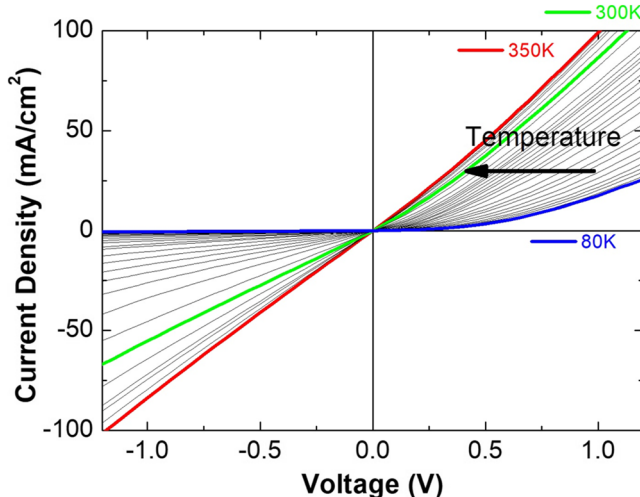
**FIGURE 13** (A) Light J-V characteristics of HeteroJunction (HJ) solar cell sample measured at different temperatures. (B) Light J-V characteristics of a homojunction solar cell sample measured at different temperatures

respect to the a-Si:H electron affinity can generate a barrier due to electron depletion of the a-Si:H layer that can extend into the c-Si substrate, leading to a nonlinear effect, which is much more evident when reducing the temperature.

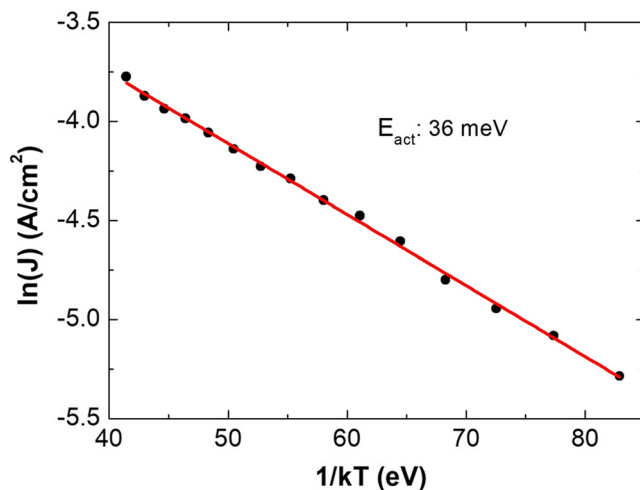
Therefore, the base contact of the cell has been physically separated from the HJ cell by removing the emitter side and contacting the c-Si wafer with a proper ohmic contact. To this purpose, samples have been appropriately prepared by removing the metal grid and the ITO of the cell side, which is not object of the test, and an ohmic contact has been produced by scratching the cell surface to penetrate the amorphous layers and by applying an Indium-Gallium eutectic.<sup>26</sup> The contact so obtained has been tested at various temperatures, verifying a linear behaviour at each temperature between 80 and 350 K. Then measurements have been performed on the c-Si/i/n-a-Si/ITO side separately, namely, on the base contact.

Figure 15 shows the dark J-V characteristics of the base contact as a function of temperature, while keeping the n-type c-Si wafer grounded. The base contact is almost ohmic only at moderate temperature (350 K; red line), while it nonlinearly behaves at room temperature (green line) and it is strongly rectifying at low temperature (80 K; blue line). Referring to the numerical simulation of the base contact reported in Figure 12(B), the nonlinear behaviour of the J-V curve at room temperature suggests a barrier against electron collection due to the  $\Phi_{TCO}$ , which is not eliminated just by the increase of doping of the n a-Si:H layer.

From the observation of the curve bundle as a function of temperature in Figure 15, an activation process from a nonlinear behaviour toward a linear one is evident. The activation energy ( $E_{act}$ ) of this process can be evaluated by an Arrhenius plot and a linear fit procedure of the current density data measured at a bias voltage of 0.4 V, corresponding to the forward bias working conditions of the base contact of the solar cell, as depicted in Figure 16. To get a better insight of this  $E_{act}$ , a detailed investigation has been performed with the aid of numerical simulations of the base contact in which the  $\Phi_{TCO}$



**FIGURE 15** Dark J-V characteristics of the base contact of the HJ solar cell sample measured at different temperatures



**FIGURE 16** Arrhenius plot evaluated from the J-V characteristics in Figure 15 at 0.4 V bias voltage

is varied in the range 4.0–4.6 eV, while keeping constant all the other parameters describing the base contact of the cell already seen in previous sections for the starting point HJ (green line in Figure 12(B)). For each  $\Phi_{TCO}$  value, the  $E_{act}$  has been calculated and then plotted in Figure 17. In this figure, the line at  $kT = 26$  meV, corresponding to room temperature, is depicted as a reference. The graph shows that if the  $E_{act}$  value is lower than 26 meV, the linear behaviour of the base contact can be ensured at least at room temperature or above. Instead, if the  $E_{act}$  value is higher than 26 meV, the base contact will always be affected by nonlinearity and its resistivity will be definitely lower than the expected value, taking only into account the resistivity of each layer of the base contact. This nonlinear effect is due to  $\chi$  mismatch at the TCO/a-Si:H interface.

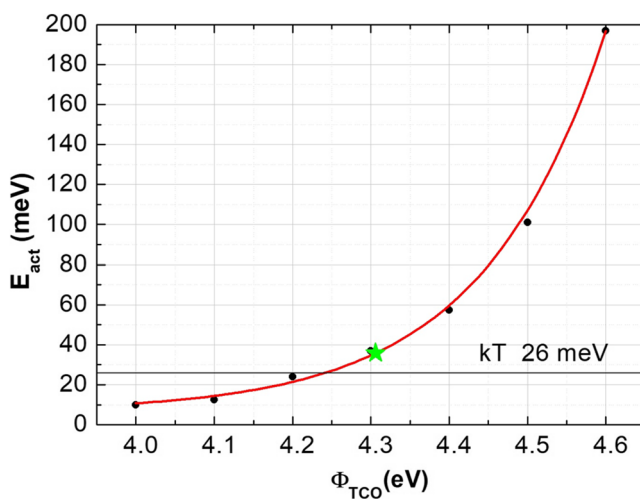


**FIGURE 17** Activation energy  $E_{act}$  of the nonlinear/linear behaviour of the J-V characteristics of HeteroJunction (HJ) base contact, calculated from simulations performed at different  $\Phi_{TCO}$  values. The green star marks the  $E_{act} = 36$  meV evaluated from the experimental data of Figure 16, referred to the HJ solar cell

The comparison between the numerical simulation and the experimental value  $E_{act} = 36$  meV reported in Figure 16 confirms that the base contact is affected by nonlinearity due to a  $\Phi_{TCO} \approx 4.3$  eV (as remarked by the green star in Figure 17), which is definitively higher than the best values. This undesired effect decreases the FF of the HJ cell. Moreover, Figure 17 gives the  $\Phi_{TCO}$  value measuring the  $E_{act}$  on the base contact of the HJ cell.

To evaluate if the nonlinear behaviour of the base contact would be sufficient to demonstrate the unexpected S-shape effect reported in Figure 13, further numerical simulations have been performed on two identical HJ cells, based on the starting point HJ, having different values of  $\Phi_{TCO}$  at the base contact and the same  $\Phi_{TCO} = 5.2$  eV at the emitter side. In Figures 18(A) and 18(B), the resulting J-V characteristics at different temperatures are shown for  $\Phi_{TCO} = 4.5$  eV and 4.1 eV, respectively. It is worth noting that in both cases, the J-V characteristics at room temperature do not show any evident S-shape; nevertheless, the cell with  $\Phi_{TCO} = 4.5$  eV shows a lower FF (81.2% vs 84.5%). When the temperature is decreased, the cell with  $\Phi_{TCO} = 4.1$  eV maintains a regular J-V curve, while the cell with  $\Phi_{TCO} = 4.5$  eV shows an onset of S-shape already at 260 K, similar to what is observed in the experimental data of a real HJ cell shown in Figure 13. The reason for this S-shape is clearly explained by the energy band distributions as obtained from the numerical simulations

reported in the bottom of Figure 18, in which the effect of the different offset at the conduction band edge at the n a-Si:H/TCO interface is evident: when the  $\Phi_{TCO}$  is 4.1 eV (b), the c-Si surface is in electron accumulation, which is an ideal situation, while if the  $\Phi_{TCO}$  is 4.5 eV (a), the c-Si surface and the n a-Si:H layer are depleted and a barrier obviously arises.

The effect of this barrier on the FF value has been analyzed in Figure 19 as a function of  $\Phi_{TCO}$  for two doped n a-Si:H layers ( $7 \times 10^{17} \text{ cm}^{-3}$  and  $1.7 \times 10^{18} \text{ cm}^{-3}$ , corresponding to  $E_d = 0.18$  eV and  $E_d = 0.14$  eV, respectively). The simulations suggest that the higher the  $\Phi_{TCO}$ , the lower the FF, and the higher the doping level, the lower the FF decrement with the  $\Phi_{TCO}$ . A higher doping can mitigate the FF reduction caused by the higher work function value, thanks to the higher carrier density, because in all the simulations, no tunnelling has been considered. Indeed, if the tunnelling mechanism were introduced, the n-a-Si:H/TCO contact would not be limited by the Schottky barrier as clearly shown by the experimental J-V characteristics of the contact reported in Figure 15.

For a n-type-doped a-Si:H layer, the FF value saturates when the  $\Phi_{TCO}$  is lower than 4.1 eV, indicating that the limiting effect of the hidden barrier is no longer influencing the cell efficiency. In conclusion, the effect of a hidden barrier at the base contact is not negligible at room temperature and represents a limiting factor for the cell FF,

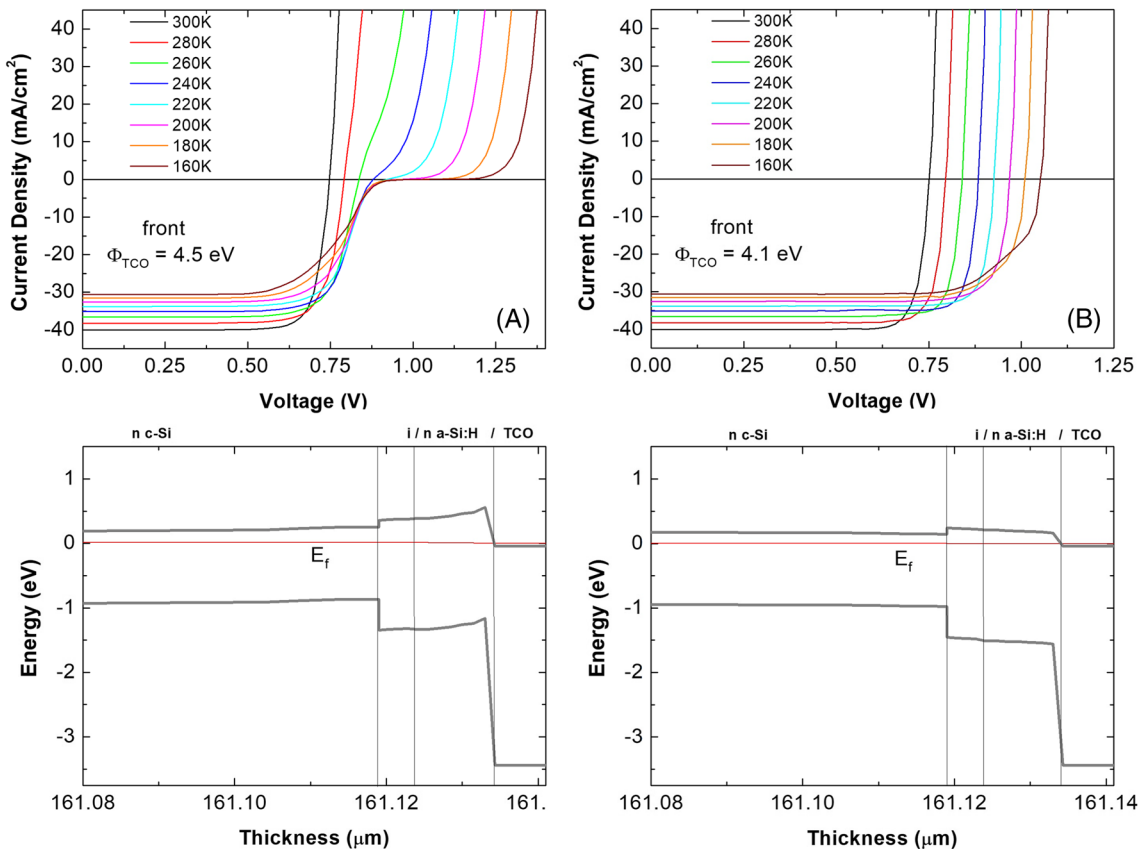


**FIGURE 18** Numerical simulation of two cells with  $\Phi_{TCO} = 5.2$  eV on the emitter and  $\Phi_{TCO} = 4.5$  eV (A) and  $\Phi_{TCO} = 4.1$  eV (B) on the base side. The J-V characteristics as a function of temperature are shown on top, the band bending simulation at 300 K in dark condition, and 0 V bias are illustrated in the bottom. The barrier at the n-aSi:H/TCO interface in (a) reflects in the S-shape and lower fill factor at room temperature

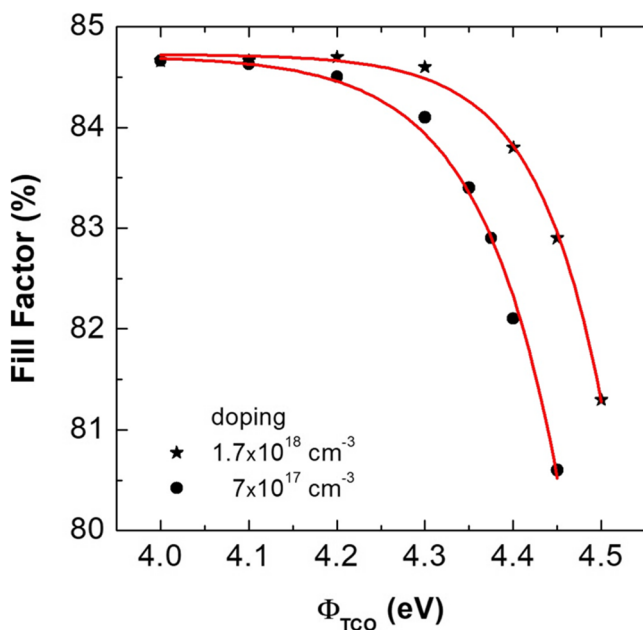


**FIGURE 19** Simulation of the trend of the fill factor as a function of  $\Phi_{TCO}$  for two different n-doped a-Si:H layers. The fill factor value saturates at 84.7% for  $\Phi_{TCO}$  below 4.1 eV

and in turn the cell efficiency, when the  $\Phi_{TCO}$  is not appropriately aligned with that of the amorphous doped layer.

At the emitter side of the HJ cell, the carrier transport is effected by a multistep tunnelling mechanism assisted by defects at the TCO/p-a-Si:H interface.<sup>27</sup> This is evident in Figure 20, where the exponential behaviour as a function of temperature of the  $J_{dark}$  of the HJ cell of Figure 13(A) measured under forward bias conditions is reported. This tunnelling mechanism relaxes the constrain of  $\Phi_{TCO}$  =

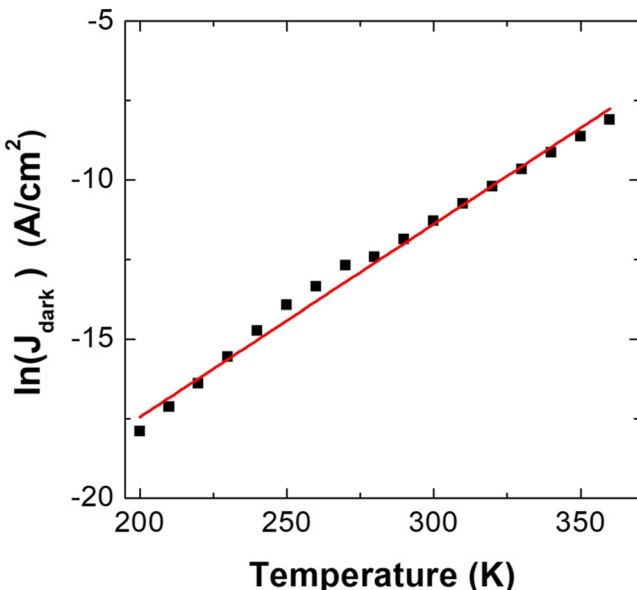


**FIGURE 20** Exponential trend of the low (0.4 V) forward bias dark current of the heteroJunction as a function of temperature, revealing a multistep tunnelling mechanism for the carrier transport

5.2 eV at the emitter side. Indeed, in practice, it is very difficult to achieve this value with conventional ITO as commonly used in the emitter side of the HJ record cell, even depositing it at room temperature. Then lower  $\Phi_{TCO}$  values can be accepted, which would not contribute to the FF lowering as reported in the literature.<sup>28</sup> For these reasons, the light J-V vs T characteristics of Figure 13(A) do not need the emitter side contribution to be simulated for the hypothesis of  $\Phi_{TCO}$  higher than 4.8 eV.

#### 4 | CONCLUSIONS

In this work, the relationship between the FF in HJ solar cells and various cell characteristics such as emitter thickness, emitter doping, density of states at interfaces, and valence band offset at the p-doped a-Si:H/i a-Si:H/n-type c-Si interfaces are deeply analyzed with the aid of numerical simulations.

It is found out that FF limitations can be due to the base contact, which is normally thought to be already optimised in HJ solar cells. With the aid of numerical simulations and appropriately designed experiments, it is shown that the  $\Phi_{TCO}$  plays a fundamental role. A misalignment between electron affinity of the a-Si:H doped layer and the TCO work function in one or both selective contacts leads to a FF reduction resulting in the generation of an unwanted S-shape, which degrades the J-V characteristic in terms of FF and  $V_{oc}$ .

Such a behaviour is evidenced on HJ solar cells by performing measurements at low temperatures. HJ cells working well at room temperature can show an S-shape at low temperatures. This is symptomatic of the presence of a hidden barrier, arising from the high value of  $\Phi_{TCO}$  at the base contact, which can result in FF values in the range of 82–83% but does not allow 85% to be achieved.

The measurement of the J-V characteristic of the base contact alone as a function of temperature confirms this assumption, showing that they switch from a quasi-linear behaviour to a rectifying one.

Different cells with different  $\Phi_{TCO}$  (from 4.1 to 4.5 eV) at the base contact have been simulated, and the activation energy values have been extrapolated and plotted as a function of  $\Phi_{TCO}$ , showing that activation energies lower than 26 meV can establish a perfect ohmic contact and the absence of any barrier limiting the FF, which corresponds to a  $\Phi_{TCO}$  for the base contact lower than 4.25 eV.

Simulations of the J-V characteristics as a function of temperature for cells having 4.1 and 4.5 eV of  $\Phi_{TCO}$  confirm the absence of S-shape in the J-V curve for the former and its presence for the latter, caused by the barrier due to the misalignment between the conduction band of n a-Si:H and the TCO. An increment of the base doping partially compensates the FF reduction, with the same TCO.

Hence, a model to predict the presence of a hidden barrier at the base contact that limits the cell fill factor has been demonstrated.

#### ACKNOWLEDGMENT

This work has received funding from the European Union's Horizon 2020 research and innovation programme under grant agreement no. 745601, AMPERE Project.

## ORCID

Luca Serenelli  <https://orcid.org/0000-0003-4584-4672>

## REFERENCES

1. Green MA, Hishikawa Y, Dunlop ED, et al. Solar cell efficiency tables (version 53). *Progress in Photovoltaics: Research and Applications*. 2019;27(1):3-12.
2. Yoshikawa K, Kawasaki H, Yoshida W, et.al. Silicon heterojunction solar cell with interdigitated back contacts for a photoconversion efficiency over 26%. *Nat Energy* 2017; 2(5): 17032.
3. Adachi D, Hernandez JL, Yamamoto K. Impact of carrier recombination on fill factor for large area heterojunction crystalline silicon solar cell with 25.1% efficiency. *Appl Phys Lett*. 2015;107(23):233506.
4. Serenelli L, Miliciani M, Izzi M, Chierchia R, Mittiga A, Tucci M. Advances in screen printing metallization for a-Si:H/c-Si heterojunction solar cells. *40th IEEE Photovoltaic Specialist Conference*, Denver, CO, 2014: 2526-2532.
5. Brendel R, Peibst R. Contact selectivity and efficiency in crystalline silicon photovoltaics. *IEEE Journal of Photovoltaics*. 2016;6(2):1413-1420.
6. Izzi M, Serenelli L, Mangiapane P, et al. Relevance of TCO work-function in n-silicon oxide emitter - c-Si (p) heterojunction solar cell. *42nd IEEE Photovoltaic Specialist Conference*, New Orleans, LA, 2015: 1-4.
7. Centurioni E, Iencinella D. Role of front contact work function on amorphous silicon/crystalline silicon heterojunction solar cell performance. *IEEE Electron Device Letters*. 2003;24(3):177-179.
8. Rößler R, Leendertz C, Korte L, Mingirulli N, Rech B. Impact of the transparent conductive oxide work function on injection-dependent a-Si:H/c-Si band bending and solar cell parameters. *J Appl Phys*. 2013; 113:144513.
9. Tucci M, Serenelli L, De Iuliis S, et al. Contact Formation on a-Si:H/c-Si heterostructure solar cells. (2012) *Physics and Technology of Amorphous-Crystalline Heterostructure Silicon Solar Cells*, van Sark W, Korte L, Roca F (eds), chap 10: 331-375, Springer. ISBN: 978-3-642-12011-4.
10. Tucci M, de Cesare G. 17% efficiency heterostructure solar cell based on p-type crystalline silicon. *J Non Cryst Solids*. 2004;338(1):663-667.
11. Tucci M, Della Noce M, Bobeico E, Roca F, De Cesare G, Palma F. Comparison of amorphous/crystalline heterojunction solar cells based on n- and p-type crystalline silicon. *Thin Solid Films*. 2004;451: 355-360.
12. Serenelli L, Izzi M, Chierchia R, Tucci M. Laser treatment to form an effective base contact in a-Si:H/c-Si heterojunction solar cells. *Energy Procedia*. 2015;84:228-235.
13. Anderson RL. Experiments on Ge-GaAs heterojunctions. *Solid-State Electronics*. 1962;5(5):341-351.
14. Menchini F, Serenelli L, Martini L, et al. Transparent hole-collecting and buffer layers for heterojunction solar cells based on n-type-doped silicon. *Applied physics. A, Materials Science & Processing*. 2018;124:489.
15. Tiedje T, Yablonoitch E, Cody GZ, Brooks BG. Limiting efficiency of silicon solar cells. *IEEE Transactions on Electron Devices*. 1984;31(5): 711-716.
16. Taguchi M, Yano A, Tohoda S, et al. 24.7% record efficiency HIT solar cell on thin silicon wafer. *IEEE Journal of Photovoltaics*. 2014;4(1): 96-99.
17. Fujiwara H, Kondo M. Interface structure in a-Si:H/c-Si heterojunction solar cells characterized by optical diagnosis technique. *4th World Conference on Photovoltaic Energy Conversion (WCPEC-7)*, Waikoloa, Hawaii, USA. 2006:1443-1448.
18. Tucci M, Serenelli L, De Iuliis S, Izzi M, de Cesare G, Caputo D. Back contact formation for p-type based a-Si:H/c-Si heterojunction solar cells. *Physica status solidi. C. Current Topics in Solid State Physics*. 2011;8:932-935.
19. Liebhaber M, Mews M, Schulze TF, Korte L, Rech B, Lips K. Valence band offset in heterojunctions between crystalline silicon and amorphous silicon (sub)oxides (a-SiO<sub>x</sub>:H, 0<x<2). *Appl Phys Lett*. 2015;106: 031601.
20. Izzi M, Tucci M, Serenelli L, et al. Doped SiO<sub>x</sub> emitter layer in amorphous/crystalline silicon heterojunction solar cell. *Applied Physics a, Materials Science & Processing*. 2014;115:705-712.
21. Ding K, Aeberhard U, Finger F, Rau U. Silicon heterojunction solar cell with amorphous silicon oxide buffer and microcrystalline silicon oxide contact layers. *Physica Status Solidi RRL*. 2012;6:193-195.
22. Ge J, Tang M, Wong J, et al. Excellent silicon surface passivation achieved by industrial inductively coupled plasma deposited hydrogenated intrinsic amorphous silicon suboxide. *International Journal of Photoenergy*. 2014;2014:752967.
23. Kern W. The evolution of silicon wafer cleaning technology. *J Electrochem Soc*. 1990;137:1887-1892.
24. Weiser G, Mell H. Temperature dependence of the optical absorption edge in a-Si:H. *J Non Cryst Solids*. 1989;114:298-300.
25. Priyanka S, Ravindra NM. Temperature dependence of solar cell performance-an analysis. *Solar Energy Materials & Solar Cells*. 2012; 101:36-45.
26. Sze SM. *Semiconductor devices, physics and technology*. New York: J. Wiley & Sons; 1985.
27. Fonash SJ. *Solar cell device physics*. New York: Academic press; 1981.
28. Ritzau KU, Bivour M, Schröer S, et al. TCO work function related transport losses at the a-Si:H/TCO-contact in SHJ solar cells. *Solar Energy Materials and Solar Cells*. 2014;131:9-13.

**How to cite this article:** Martini L, Serenelli L, Menchini F, Izzi M, Tucci M. Silicon heterojunction solar cells toward higher fill factor. *Prog Photovolt Res Appl*. 2020;1-14. <https://doi.org/10.1002/pip.3241>